Flexomagnetic response of nanostructures

Sai Sidhardh, and M. C. Ray

Citation: Journal of Applied Physics **124**, 244101 (2018); doi: 10.1063/1.5060672
View online: https://doi.org/10.1063/1.5060672
View Table of Contents: http://aip.scitation.org/toc/jap/124/24
Published by the American Institute of Physics

Flexomagnetic response of nanostructures

Sai Sidhardh and M. C. Ray[a)]
Department of Mechanical Engineering, Indian Institute of Technology Kharagpur, Kharagpur 721302, India

(Received 21 September 2018; accepted 2 December 2018; published online 26 December 2018)

This paper presents the constitutive modeling of the flexomagnetic (FM) effect in structures involving a non-zero magnetic field generated in the presence of inhomogeneous strain across the domain. In order to evaluate the magneto-elastic (ME) structural response, the tensorial governing equations and associated boundary conditions for the mechanical and magnetic variables are derived here using the variational principle. Following this, these differential equations are solved to determine the effect of FM over the bending response of a cantilever piezomagnetic nanobeam. Different magnetic boundary conditions are analyzed to study the effect of direct and converse FM couplings over the ME response. The significant influence of FM coupling over the ME response has been noted for thin beams with low-dimensions, which wanes as the geometric dimensions are increased. Given the significance of this size-dependent FM response in nano-structures, the theory for flexomagnetism proposed here may be utilized in the development of smart ME nano-structures with the potential for wide applications. *Published by AIP Publishing.* https://doi.org/10.1063/1.5060672

I. INTRODUCTION

With the developments in nanotechnology progressing at a rapid pace, the increase in the applications using micro- and nano-electromechanical systems (MEMs/NEMs) may be noted. However, the classical theories of elasticity applicable at the macroscale do not predict the elastic response at this scale satisfactorily. At this scale, given the low-dimensions of these structures, experiments have demonstrated the significant effect of strain gradients on the elastic response.[1–3] The importance of these gradients toward determining the response of the structures has led to the formulation of strain gradient elasticity (SGE) theories.[4,5]

Furthermore, it has been observed that a non-zero electrical field is induced in a dielectric in the presence of non-uniform strains. This coupling of the electric field and strain gradient is referred to as the flexoelectric effect. This coupling was theoretically studied in crystals almost 50 years ago.[6–8] Experimental studies were carried out by Cross and coworkers over a number of dielectrics to evaluate the corresponding coefficients.[9–14] These experiments have been carried out by investigating the bending deformation of structures, given the large strain gradients (flexure) generated by this deformation. Extensive theoretical studies have also been carried out to analyze the flexoelectric effects in solids, and the development of actuators, sensors, and energy harvesters from such structures.[15–34]

As discussed above, the major section of the literature available on strain gradients is devoted to either strain gradient elasticity or the flexoelectric phenomenon. However, magneto-elastic (ME) coupling in crystals, in the form of a correlation between the strain gradient and the induced magnetic fields, is relatively unexplored. This coupling induces a non-zero magnetic field in the presence of in-homogeneous strains and is referred to as the *flexomagnetic* (FM) effect. This may be considered as a component of the more general flexomagnetoelectric effect, coined by Bobylev and Pikin[35] to study the coupling of magneto-electric and elastic responses in liquid crystals. Such studies in multiferroics generally analyzed the converse effect of the electro-magnetic field over the molecular reorientations.[36] The ME linear coupling of strain-gradient with the magnetic field is incorporated by an addition of the associated coupling energy to the total free energy of a ferroelectric.[37] A similar approach has been adopted for the development of a general expression of the total free energy for a ME solid, including the flexo- and piezo- electromagnetic effects, and the non-linear electro- and magneto-strictions.[38,39]

Unlike the more commonly analyzed piezomagnetic (PM) effect, which provides a coupling of the strain and magnetic fields, flexomagnetism involving strain gradients is ignored owing to its negligible effect in the macro-structures. However, due to the dimensional scaling exhibited by the strain gradients, the FM effect gains significance as the geometric dimensions of the structure approach micro- and nano-scales. Moreover, the PM effect is severely restricted by the crystal symmetries. Eliseev *et al.*[40–42] carried out extensive theoretical calculations for evaluating the form of the FM tensor in various magnetic classes using the symmetry theory. It has been suggested that all the 90 magnetic classes exhibit a non-zero FM effect, at least close to the surface. Lukashev *et al.* carried out studies over Mn-based antiperovskites to evaluate the coefficients of this coupling tensor from first principles.[43,44] Therefore, a non-zero magnetic field may be induced in such solids by the FM coupling. This indicates the potential for the development of piezomagnetic-like structures without the use of any conventional piezomagnetic materials.

Most of the literature cited above on the FM is restricted to studying this effect over a scale of few crystals, with only some of them focusing on flexo-coupling in structures like

[a)]Author to whom correspondence should be addressed: mcray@mech.iitkgp.ernet.in

disks and cylinders.[41] However, no such analysis has been carried for evaluating the FM effects over the deformation of a more general structure like a beam, where high strain gradients can be produced upon bending, as discussed above. Also, a clear description of the constitutive relations for the ME variables along with the three-dimensional governing equations and the associated boundary conditions for these variables has not been provided in the literature. They would be necessary to determine the multi-field response of the FM structure. Thus, we intend to present here the constitutive relations and derive the necessary governing equations and boundary conditions using the variational principles from the total free energy provided in the literature.[40] Furthermore, this paper will analyze the effect of flexomagnetic coupling over the magneto-elastic response for the bending deformation of a piezo-magnetic beam. In studies pertaining to the nanostructures, where the ratio of the surface area to volume is non-trivial, additional energy pertaining to the free surfaces of the solid may also be considered. Some of the common examples of the effects caused by such energies are the "surface elasticity," "surface piezoelectricity," and "surface flexoelectricity."[45] However, the objective of the current study is to analyze the flexomagnetic response over nanostructures. Thus, the energy corresponding to such surface effects will not be considered in the current study.

II. MODELING FLEXOMAGNETIC RESPONSE

A. Constitutive relations

The free energy density $\mathcal{U}$ of a non-centrosymmetric ferromagnetic exhibiting the piezomagnetic (PM) and the flexomagnetic (FM) effects has been evaluated using the Landau-Ginsburg-Devonshire (LGD) phenomenological approach.[46] The expression for this free energy density may be expressed in terms of the second order strain tensor $\boldsymbol{\epsilon}$, third order strain gradient tensor $\boldsymbol{\eta}$, and the magnetic field vector $\boldsymbol{H}$ as follows:[40,41]

$$\mathcal{U}(\boldsymbol{\epsilon},\boldsymbol{\eta},\boldsymbol{H}) = -\frac{1}{2}\boldsymbol{H}\cdot\boldsymbol{a}\cdot\boldsymbol{H} + \frac{1}{2}\boldsymbol{\epsilon}:\boldsymbol{C}:\boldsymbol{\epsilon} + \frac{1}{2}\boldsymbol{\eta}\vdots\boldsymbol{g}\vdots\boldsymbol{\eta} + \boldsymbol{\epsilon}:\boldsymbol{r}\vdots\boldsymbol{\eta} - \boldsymbol{H}\cdot\boldsymbol{d}:\boldsymbol{\epsilon} - \boldsymbol{H}\cdot\boldsymbol{\mu}\vdots\boldsymbol{\eta}, \tag{1}$$

where given a displacement field vector $\boldsymbol{u}$, the strain and strain gradient tensors are defined as

$$\boldsymbol{\epsilon} = \frac{1}{2}(\nabla\otimes\boldsymbol{u} + \boldsymbol{u}\otimes\nabla), \quad \boldsymbol{\eta} = \boldsymbol{\epsilon}\otimes\nabla \tag{2}$$

and the magnetic field vector $\boldsymbol{H}$ is expressed in terms of the magnetic potential ψ as follows:[47,48]

$$\boldsymbol{H} = -\nabla\psi. \tag{3}$$

The above definition for the magnetic potential is based on the assumption that the circulation of the magnetic field (curl $\boldsymbol{H} = 0$) around a closed contour enclosing the solid being zero. The above result is applicable only if this contour does not enclose any distribution of current, from either external or internal sources.[37] With the net contribution of the magnetization toward the current being zero, we assume that no external stationary currents are present in the ME solid being analyzed here.

In the expression for free energy density given by Eq. (1), $\boldsymbol{a}$ is the second order magnetic permeability tensor, $\boldsymbol{C}$ is the fourth-order classical elasticity coefficient tensor, and $\boldsymbol{g}$ is the sixth-order gradient elasticity coefficient tensor. The fifth-order tensor $\boldsymbol{r}$ couples the strain and strain-gradient tensors and is non-zero only for the non-centrosymmetric solids. The energy corresponding to the tensors $\boldsymbol{g}$ and $\boldsymbol{r}$ is incorporated in the free energy density given in Eq. (1) due to the significance of SGE for structures at micro- and nano-scales.[49] Furthermore, the necessity of including the SGE in such multifield studies is to avoid inconsistent boundary conditions, as discussed by Yurkov for flexoelectric solids.[50] The third-order tensor $\boldsymbol{d}$ may be referred to as the *piezomagnetic* tensor coupling the magnetic field vector and the elastic strain. As mentioned previously, this odd-ordered tensor is non-zero only for a non-centrosymmetric crystal solid. Finally, the fourth-order $\boldsymbol{\mu}$ tensor coupling the strain gradient and the magnetic field is called the *flexomagnetic* tensor. This flexomagnetic tensor may be considered as an equivalent form of the fourth-order flexomagnetic coupling tensor Q^m provided by Eliseev *et al.*[40] and is obtained from a Legendre transform of the free-energy given in Eq. (1) with respect to the magnetic variables.[51] The tensor Q^m couples the magnetization vector and strain gradient tensor, and the complete form of this tensor may be obtained from studies carried out by Eliseev *et al.* over the form of Q^m for all the magnetic classes.[40] Unlike piezomagnetism, flexomagnetism is also exhibited by the centrosymmetric ferroics where the piezomagnetic tensor $\boldsymbol{d}$ would be zero, thereby indicating the presence of a non-zero magneto-elastic coupling in all crystalline structures irrespective of their symmetry.

Considering the variables $\boldsymbol{\epsilon}$, $\boldsymbol{\eta}$, and $\boldsymbol{H}$, the constitutive relations may be expressed as[40]

$$\boldsymbol{\sigma} = \frac{\partial U}{\partial \boldsymbol{\epsilon}} = \boldsymbol{C}:\boldsymbol{\epsilon} + \boldsymbol{r}\vdots\boldsymbol{\eta} - \boldsymbol{H}\cdot\boldsymbol{d}, \tag{4a}$$

$$\boldsymbol{\tau} = \frac{\partial U}{\partial \boldsymbol{\eta}} = \boldsymbol{g}:\boldsymbol{\eta} + \boldsymbol{\epsilon}:\boldsymbol{r} - \boldsymbol{H}\cdot\boldsymbol{\mu}, \tag{4b}$$

$$\boldsymbol{B} = -\frac{\partial U}{\partial \boldsymbol{H}} = \boldsymbol{a}\cdot\boldsymbol{H} + \boldsymbol{d}:\boldsymbol{\epsilon} + \boldsymbol{\mu}\vdots\boldsymbol{\eta}. \tag{4c}$$

In the above relations, the second-ordered Cauchy-stress tensor $\boldsymbol{\sigma}$, the third-order higher-order stress tensor $\boldsymbol{\tau}$, and the magnetic flux vector (also called the magnetic induction vector) $\boldsymbol{B}$ are the energy-conjugates of $\boldsymbol{\epsilon}$, $\boldsymbol{\eta}$, and $\boldsymbol{H}$, respectively. Similar to the piezomagnetic behavior, the effect of the flexomagnetic tensor $\boldsymbol{\mu}$ over the magnetic field in Eq. (4c) will be referred to as the direct flexomagnetic behavior, and the effect of $\boldsymbol{\mu}$ over the mechanical higher order stress in Eq. (4b) will be referred to as the converse flexomagnetic effect. Therefore, a non-uniform strain causing a magnetic flux to be *induced* across the domain will be referred to as the *direct* flexomagnetic effect. Furthermore, a non-uniform strain *developed* across the domain in the presence of

magnetic field is the *converse* flexomagnetic effect. Overall, for centrosymmetric crystals with $\boldsymbol{d} = 0$, a non-zero $\boldsymbol{\mu}$ provides the ME coupling in non-piezomagnetic materials.

B. Governing equations

The governing equations and the associated boundary conditions necessary for determining the magneto-elastic response of a flexomagnetic structure may be obtained by applying the variational principle over $\mathcal{U}$. The first variation of the total free energy over a volume Ω may be written for the free energy density given in Eq. (1) using the constitutive relations given above as follows:

$$\delta\mathcal{W}(\boldsymbol{\epsilon}, \boldsymbol{\eta}, \boldsymbol{H}) = \int_{\Omega} \boldsymbol{\sigma}:\delta\boldsymbol{\epsilon} + \boldsymbol{\tau}\vdots\delta\boldsymbol{\eta} - \boldsymbol{B}\cdot\delta\boldsymbol{H}dV. \tag{5}$$

The above variation is carried out in terms of the independent variations of the displacements, normal gradients of the displacements, and magnetic potential. Consider an external work $\delta\mathcal{V}$ applied over the system as follows:

$$\delta\mathcal{V} = \int_{\Omega} \bar{\boldsymbol{b}}\cdot\delta\boldsymbol{u}dV + \int_{\partial\Omega} \bar{\boldsymbol{t}}\cdot\delta\boldsymbol{u}dA + \int_{\partial\Omega} \bar{\boldsymbol{q}}\cdot\boldsymbol{n}\cdot(\delta\boldsymbol{u}\otimes\nabla)dA + \oint_{\Gamma} \bar{\boldsymbol{e}}\cdot\delta\boldsymbol{u}dl, \tag{6}$$

where $\bar{\boldsymbol{b}}$, $\bar{\boldsymbol{t}}$, $\bar{\boldsymbol{q}}$, and $\bar{\boldsymbol{e}}$ are the prescribed values of the distributed mechanical forces over the volume Ω, smooth surface $\partial\Omega$, and edges Γ. $\boldsymbol{n}$ is the unit normal vector over smooth surface $\partial\Omega$. The variational principle $\delta\mathcal{W} = \delta\mathcal{V}$ gives the following governing differential equations:

$$\partial\boldsymbol{u}: \quad -\nabla\cdot(\boldsymbol{\sigma} - \nabla\cdot\boldsymbol{\tau}) = \bar{\boldsymbol{b}} \quad \text{in } \Omega, \tag{7a}$$

$$\partial\psi: \quad \nabla\cdot\boldsymbol{B} = 0 \quad \text{in } \Omega. \tag{7b}$$

Equation (7b) is Maxwell's equation, commonly referred to as Gauss's law for magnetism, which is obtained here from variational principles by an independent variation of the magnetic potential across the domain. In this derivation, an assumption regarding the absence of magnetic monopoles in the domain has been made. The associated boundary conditions obtained from the variational principle may be expressed as

$$\boldsymbol{n}\cdot(\boldsymbol{\sigma} - \nabla\cdot\boldsymbol{\tau}) - [\boldsymbol{R}:(\boldsymbol{n}\cdot\boldsymbol{\tau})\otimes\nabla] + [\boldsymbol{R}:(\nabla\otimes\boldsymbol{n})][(\boldsymbol{n}\otimes\boldsymbol{n}):\boldsymbol{\tau}] = \bar{t} \quad \text{or} \quad \boldsymbol{u} = \bar{\boldsymbol{u}} \quad \text{on } \partial\Omega, \tag{8a}$$

$$(\boldsymbol{n}\otimes\boldsymbol{n}):\boldsymbol{\tau} = \bar{q}, \text{ or } \delta\boldsymbol{u}\otimes\nabla = \delta\bar{\boldsymbol{u}}\otimes\nabla \quad \text{on } \partial\Omega, \tag{8b}$$

$$[[\boldsymbol{m}\cdot(\boldsymbol{n}\cdot\boldsymbol{\tau})]] = \bar{e}, \text{ or } \boldsymbol{u} = \bar{\boldsymbol{u}} \quad \text{on } \Gamma, \tag{8c}$$

$$\boldsymbol{n}\cdot\boldsymbol{B} = 0, \quad \text{or} \quad \psi = \bar{\psi} \quad \text{on } \partial\Omega, \tag{8d}$$

where $\bar{u}$ and $\bar{\psi}$ are the prescribed values for the displacement vector and applied magnetic potential at the surface $\partial\Omega$ and edges Γ. In the above equations, $\boldsymbol{R}$ is the second-ordered surface projection tensor defined as $\boldsymbol{R} = \boldsymbol{I} - \boldsymbol{n}\otimes\boldsymbol{n}$, with $\boldsymbol{I}$ being a second-ordered identity tensor, $\boldsymbol{m}$ is the co-normal vector to the tangent along the sharp edge Γ and normal to the surface $\boldsymbol{n}$,[46] and $[[\cdot]]$ notation is used to denote a jump across the sharp edge Γ. The governing differential equation and associated boundary conditions for the variation of the mechanical displacement $\boldsymbol{u}$, given above, are identical to that obtained for a strain gradient elastic solid.[49] A detailed derivation of the same has been carried out in the literature[49] and hence not presented here for the sake of brevity.

Therefore, in this section, we have introduced the free energy corresponding to a ferroic structure exhibiting the PM and FM effects, while also considering the SGE. Subsequently, the constitutive relations for such a material have been provided in Eq. (4). The ME response of the structure may be evaluated from solving the governing differential equations given in Eq. (7), together with the associated boundary conditions provided in Eq. (8). In Sec. III, we intend to present a case-study of ferroic beams and study the effect of FM on its ME response.

III. BENDING RESPONSE OF ME BEAMS

A schematic of the cantilever ferroic nanobeam considered for the current study is illustrated in Fig. 1. As shown in the figure, the geometric length and the height of the beam are denoted by L and h, respectively. The width of the beam will always be maintained as $b = 2\times h$. The Cartesian coordinate system chosen for the current study is also shown in the schematic. The x_1-axis lies along the mid-plane across the length of the undeformed beam such that $x_1 = 0$ and $x_1 = L$ correspond to the ends of the beam. The x_3-axis lies transverse to x_1, along the thickness of the beam. Therefore, $x_3 = \pm h/2$ are the top and bottom surfaces of the beam. The origin is chosen at the left end of the beam as shown in the figure.

The boundary conditions corresponding to the magnetic field may be chosen in order to exhibit the direct or converse

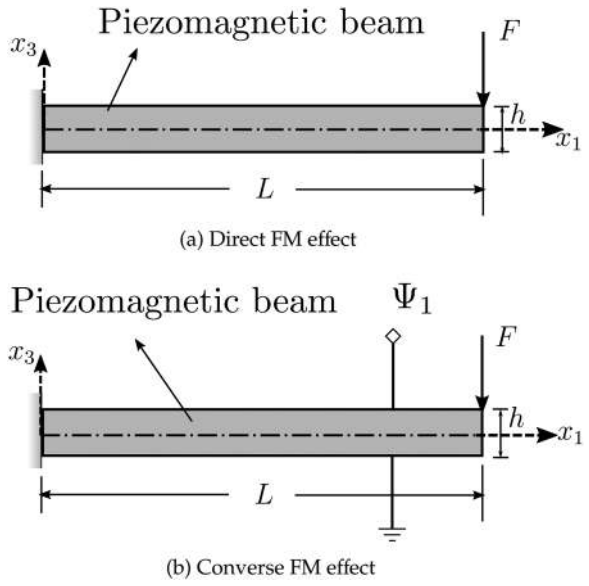

FIG. 1. Schematic of a cantilever piezomagnetic beam indicating the configurations for (a) direct FM effect and (b) converse FM effect, along with the Cartesian coordinate system chosen for this study.

FM effects. The configuration of the beam in both these conditions is illustrated in Fig. 1. The bending response of ME beams considering the two magnetic boundary conditions will be evaluated separately here.

For the current study, the Euler-Bernoulli (E-B) beam displacement hypothesis will be used to evaluate the mechanical response. According to the Euler-Bernoulli beam theory, the components of the displacement field $\boldsymbol{u}(\boldsymbol{x})$ are given by

$$u_1(x_1, x_3) = u(x_1) - x_3 \frac{dw(x_1)}{dx_1}, \quad u_3(x_1, x_3) = w(x_1), \tag{9}$$

where $u(x_1)$ and $w(x_1)$ are the axial and transverse displacements of the mid-plane of the beam, respectively. The rationale behind the choice of this hypothesis for the current study will be provided later. The only non-zero component of the strain tensor ϵ_{11}, and its gradients along x_1 and x_3 evaluated using the definitions given in Eq. (2) are given as

$$\begin{aligned} &\epsilon_{11} = \frac{du}{dx_1} - x_3 \frac{d^2w}{dx_1^2}, \quad \eta_{111} = \frac{d^2u}{d^2x_1} - x_3 \frac{d^3w}{dx_1^3}, \\ &\eta_{311} = -\frac{d^2w}{dx_1^2}. \end{aligned} \tag{10}$$

In general, the E-B theory presented above is suitable for slender structures with the length of the beam atleast an order greater than the transverse thickness. Thus, the axial gradient of the strain η_{111} $(=\epsilon_{11,1})$ may be neglected in comparison with its transverse gradient η_{311} $(=\epsilon_{11,3})$. Therefore, for all the cases studied henceforth η_{111} is neglected.

Also, given the slender beam assumption, the gradient of the magnetic potential ψ across the length is also negligible when compared to its variation across the thickness.[52] Thus, the in-plane magnetic field can be neglected here. This is analogous to the consideration of a non-zero transverse electrical field E_3, while neglecting the axial electrical field E_1 in slender piezoelectric and flexoelectric beams.[16,21,53] Thus, only the H_3 component will be considered for the current study.

The total strain energy including the SGE from Eq. (1) involves the $\boldsymbol{C}$, $\boldsymbol{r}$, and $\boldsymbol{g}$ tensors.

For the current study involving non-centrosymmetric orthotropic ferroics, the fifth-ordered $\boldsymbol{r}$ and the sixth-ordered $\boldsymbol{g}$ tensors need to be evaluated. However, only a limited literature is available on these tensors for different crystal and elastic symmetries. Thus, the strain gradient elasticity tensor $\boldsymbol{g}$ is evaluated using the definitions for isotropic centrosymmetric structures provided by Mindlin[4] and Mindlin and Eshel,[5] and the strain-strain gradient coupling tensor $\boldsymbol{r}$ is ignored here. This is an assumption used here due to the lack of proper models for evaluating these tensors. A sixth-order gradient elasticity coefficient tensor $\boldsymbol{g}$ derived by Zhou *et al.* for a linear elastic, isotropic, and centrosymmetric solid involving three independent material constants, also referred to as the generalized first strain theory of elasticity, is given as[54]

$$\begin{aligned} g_{ijklmn} = {} & g_1\left[(\delta_{ij}\delta_{kl} + \delta_{ik}\delta_{jl})\delta_{mn} + (\delta_{im}\delta_{ln} + \delta_{in}\delta_{lm})\delta_{jk}\right] + g_2\left[\delta_{ij}(\delta_{km}\delta_{ln} + \delta_{kn}\delta_{lm}) + \delta_{ik}(\delta_{jm}\delta_{ln} + \delta_{jn}\delta_{lm})\right] \\ & g_3\delta_{il}\delta_{jk}\delta_{mn} + g_4\delta_{il}(\delta_{jm}\delta_{kn} + \delta_{jn}\delta_{km}) + g_5\left[\delta_{im}(\delta_{jn}\delta_{kl} + \delta_{jl}\delta_{kn}) + \delta_{in}(\delta_{jm}\delta_{kl} + \delta_{jl}\delta_{km})\right]. \end{aligned} \tag{11}$$

Here, μ is the shear modulus (which is a scalar, unlike the flexomagnetic coupling tensor $\boldsymbol{\mu}$). The five material constants g_i $(i = 1, 2, \ldots, 5)$ are expressed in terms of the Lamé parameter μ, and the material length scales l_0, l_1, and l_2 as follows:[54]

$$\begin{aligned} &g_1 = -\frac{2}{3}(g_2 + g_5), \quad g_3 = \frac{8}{3}g_2 + \frac{2}{3}g_5, \\ &g_2 = \frac{\mu}{30}(27l_0^2 - 4l_1^2 - 15l_2^2), \quad g_4 = \frac{\mu}{3}(l_1^2 + 6l_2^2), \\ &g_5 = \frac{\mu}{3}(l_1^2 - 3l_2^2). \end{aligned} \tag{12}$$

Thus, using the expressions for the strain, strain-gradients derived from Euler-Bernoulli hypothesis, and the transverse magnetic field in the tensorial form of the constitutive relations given in Eq. (4), we get the following relations:

$$\begin{aligned} &\sigma_{11} = C_{11}\epsilon_{11} - d_{31}H_3, \quad \tau_{311} = g_{31}\eta_{311} - \mu_{31}H_3, \\ &B_3 = a_{33}H_3 + d_{31}\epsilon_{11} + \mu_{31}\eta_{311}. \end{aligned} \tag{13}$$

In the above expressions, Voigt's notation has been used to simplify the representation as $C_{11} = C_{1111}$, $d_{31} = d_{311}$, $\mu_{3311} = \mu_{31}$. Also, for simplicity, we have used $g_{31} = g_{311311}$, which may be evaluated from Eq. (11) to be $g_{311311} = g_3 + 2g_4$. The Euler-Bernoulli displacement hypothesis is used here owing to the lack of the literature on the evaluation of complete flexomagnetic tensor $\boldsymbol{\mu}$. In the studies by Eliseev *et al.*[40] and Lukashev and Sabirianov,[43] only a single value for the $\boldsymbol{\mu}$ has been evaluated from the first principle studies. We assume this value to be equal to μ_{31} with sufficient modifications owing to the difference of independent variables used in energy functional here [Eq. (1)]. The use of any higher theory for displacement to model the gradients comprehensively will invariably require more than one component of the FM tensor, where the relative ratios of these components will significantly determine the ME response. Considering that the objective of the current study is to provide a phenomenological study of the FM effect in ME beams, the Euler-Bernoulli beam theory has been used here, much alike the studies involving flexoelectricity.[16,21,33]

The variation of free energy density $\delta\mathcal{W}$ over Ω given in Eq. (5) may be simplified for the current study using the

components in Eq. (13) as follows:

$$\delta\mathcal{W} = \int_{\Omega} \sigma_{11}\delta\epsilon_{11} + \tau_{311}\delta\eta_{311} - B_3\delta H_3 dV. \tag{14}$$

Using Eqs. (3) and (10), we can simplify the above expression in terms of the independent variations of $u(x_1)$, $w(x_1)$, and $\psi(x_1, x_3)$ as follows:

$$\begin{aligned}\delta\mathcal{W} = &-\int_{x_1=0}^{L} N_{11,1}\delta u dx_1 - \int_{x_1=0}^{L}(M_{11,11} + T_{311,11})\delta w dx_1 - \int_{x_1=0}^{L}\int_{x_3=-h/2}^{h/2} B_{3,3}\delta\psi dx_3 dx_1 + \left[N_{11}\delta u\right]_{x_1=0}^{x_1=L} \\ &+ \left[(M_{11,1} + T_{311,1})\delta w\right]_{x_1=0}^{x_1=L} - \left[(M_{11} + T_{311})\frac{d\delta w}{dx_1}\right]_{x_1=0}^{x_1=L} + \int_{x_1=0}^{L}\left[B_3\delta\psi\right]_{x_3=-h/2}^{x_3=h/2} dx_1,\end{aligned} \tag{15}$$

where the stress resultants N_{11}, M_{11}, and T_{311} are defined as follows:

$$\begin{aligned} N_{11} &= \int_{x_3=-h/2}^{x_3=h/2} \sigma_{11} dx_3, \quad M_{11} = \int_{x_3=-h/2}^{x_3=h/2} x_3\sigma_{11} dx_3, \\ T_{311} &= \int_{x_3=-h/2}^{x_3=h/2} \tau_{311} dx_3. \end{aligned} \tag{16}$$

From the variational principle, the mechanical governing differential equations are given as follows:

$$\delta u: \quad N_{11,1} = 0, \quad \delta w: \quad M_{11,11} + T_{311,11} = 0 \text{ in } \Omega \tag{17}$$

and the essential and natural boundary conditions are given as

$$N_{11} = F_a \quad \text{or} \quad \delta u = 0 \quad \text{at} \quad x_1 = 0, L, \tag{18a}$$

$$M_{11,1} + T_{311,1} = F_t \quad \text{or} \quad \delta w = 0 \quad \text{at} \quad x_1 = 0, L, \tag{18b}$$

$$M_{11} + T_{311} = M_b \quad \text{or} \quad \frac{d\delta w}{dx_1} = 0 \quad \text{at} \quad x_1 = 0, L. \tag{18c}$$

Here, F_a, F_t, and M_b are the axial force, transverse force, and bending moment applied at the longitudinal ends of the beam, respectively. Furthermore, from Eq. (15), the governing differential equation corresponding to magnetic variables may be expressed as

$$\delta\psi: \quad B_{3,3} = 0 \quad \text{in } \Omega, \tag{19}$$

with the associated boundary conditions throughout the length of the beam being given as

$$\text{either } B_3 = 0 \quad \text{or} \quad \psi = \overline{\psi} \quad \text{for} \quad x_3 = \pm\frac{h}{2}. \tag{20}$$

We begin by solving the differential equation given in Eq. (19), to determine the magnetic fields in terms of the mechanical displacements. Thereafter, the mechanical governing equations are solved using these results, for the magnetic fields, to obtain the axial and transverse displacement components. The differential equations in Eq. (19) will be solved for the two different prescribed boundary conditions of the magnetic field given in Eq. (20). It may be noted that the condition $B_3 = 0$ at $x_3 = \pm h/2$ is used for estimating the induced magnetic potential and may be treated as the direct FM effect. On the other hand, satisfying the prescribed values of magnetic potential $\overline{\psi}$ at $x_3 = \pm h/2$ is analogous to studying the effect of applying a voltage over a piezoelectric structure. This may be treated as the converse FM effect.

A. Direct FM effect

It is obvious that the solution for the magnetic governing equation given by Eq. (19) satisfying the natural boundary condition given by Eq. (20) is

$$B_3 = 0 \quad \text{throughout the domain } \Omega. \tag{21}$$

Using the constitutive relation for $\boldsymbol{B}$ given in Eq. (13), definitions of the strain and strain gradients in Eq. (10), and the magnetic field in Eq. (3), we obtain the magnetic potential ψ in terms of the displacement gradients as follows:

$$\psi = \frac{1}{a_{33}}\left(d_{31}\frac{du}{dx_1} - \mu_{31}\frac{d^2w}{dx_1^2}\right)x_3 - \frac{x_3^2}{2}\frac{d_{31}}{a_{33}}\frac{d^2w}{dx_1^2} + C_0, \tag{22}$$

where C_0 is any arbitrary constant. The magnetic potential difference across the transverse surfaces $\Delta\psi$ $(= \psi|_{x_3=h/2} - \psi|_{x_3=-h/2})$ may be evaluated to be

$$\Delta\psi = h\frac{1}{a_{33}}\left(d_{31}\frac{du}{dx_1} - \mu_{31}\frac{d^2w}{dx_1^2}\right). \tag{23}$$

Using the magnetic potential derived in Eq. (22) in the definition for H_3, we get

$$H_3 = -\frac{d_{31}}{a_{33}}\left(\frac{du}{dx_1} - x_3\frac{d^2w}{dx_1^2}\right) + \frac{\mu_{31}}{a_{33}}\frac{d^2w}{dx_1^2}. \tag{24}$$

Using the above result for H_3, the solution for the bending response of the ferroic nanobeams in the case of the direct FM effect may be obtained from solving the mechanical governing equations given in Eq. (17). The Cauchy and the higher order stresses, for the above magnetic field, determined from

the constitutive relations given in Eq. (13) are

$$\sigma_{11} = \left(C_{11} + \frac{(d_{31})^2}{a_{33}}\right)\left(\frac{du}{dx_1} - x_3\frac{d^2w}{dx_1^2}\right) - \frac{\mu_{31}d_{31}}{a_{33}}\frac{d^2w}{dx_1^2},$$
$$\tau_{311} = \frac{\mu_{31}d_{31}}{a_{33}}\left(\frac{du}{dx_1} - x_3\frac{d^2w}{dx_1^2}\right) - \left(g_{31} + \frac{(\mu_{31})^2}{a_{33}}\right)\frac{d^2w}{dx_1^2}. \tag{25}$$

The stress resultants N_{11}, M_{11}, and T_{311} derived by using the expressions for stresses given above in Eq. (16) are

$$N_{11} = A_f\left(C_{11} + \frac{(d_{31})^2}{a_{33}}\right)\frac{du}{dx_1} - A_f\frac{\mu_{31}d_{31}}{a_{33}}\frac{d^2w}{dx_1^2},$$
$$M_{11} = -I_f\left(C_{11} + \frac{(d_{31})^2}{a_{33}}\right)\frac{d^2w}{dx_1^2}, \tag{26}$$
$$T_{311} = A_f\frac{\mu_{31}d_{31}}{a_{33}}\frac{du}{dx_1} - A_f\left(g_{31} + \frac{(\mu_{31})^2}{a_{33}}\right)\frac{d^2w}{dx_1^2},$$

where $A_f = b \times h$ is the area of the cross section for the beam and $I_f = bh^3/12$ is its second moment of area. Substituting these resultants in the governing equations given in Eq. (17) provides the following simultaneous system of differential equations in axial and transverse displacements

$$A^{DFM}\frac{d^2u}{dx_1^2} - B^{DFM}\frac{d^3w}{dx_1^3} = 0,$$
$$-D^{DFM}\frac{d^4w}{dx_1^4} + B^{DFM}\frac{d^3u}{dx_1^3} = 0, \tag{27}$$

where A^{DFM} is the effective axial rigidity, D^{DFM} is the effective bending rigidity, and B^{DFM} is the bending-extension coupling coefficient of the FM beam under the direct FM effect. These coefficients are given by

$$A^{DFM} = A_f\left(C_{11} + \frac{(d_{31})^2}{a_{33}}\right), \quad B^{DFM} = A_f\frac{\mu_{31}d_{31}}{a_{33}},$$
$$D^{DFM} = I_f\left(C_{11} + \frac{(d_{31})^2}{a_{33}}\right) + A_f\left(g_{31} + \frac{(\mu_{31})^2}{a_{33}}\right). \tag{28}$$

From the definition of B^{DFM} it may be importantly noted that the bending-extension coupling is exhibited here due to the *simultaneous* consideration of piezomagnetism and flexomagnetism effects.

The effect of SGE in increasing the bending rigidity by a factor $A_f g_{31}$ must be noted. However, having the strain gradient η_{111} neglected, the axial rigidity A^{DFM} is unaffected by the SGE.

The PM and FM couplings result in a change of the bending rigidity as seen from the expression for D^{DFM} in Eq. (28). The ratio of the contributions of FM and PM coupling toward the bending rigidity may be expressed as

$$\frac{D_{FM}^{DFM}}{D_{PM}^{DFM}} = \frac{A_f\frac{(\mu_{31})^2}{a_{33}}}{I_f\frac{(d_{31})^2}{a_{33}}} \propto \left(\frac{\mu_{31}}{h \times d_{31}}\right)^2. \tag{29}$$

Here the inverse proportionality to geometric height indicates the size-dependence of the FM behavior. The FM effect will gain significance in structures of low-dimensions where the above ratio is not negligible. From the material properties provided in the numerical studies of Sec. IV, for $\mu_{31} = 10^{-10}$ N/A, this ratio would be significant only for sub-nanoscale dimensions.

The associated mechanical boundary conditions from Eq. (18) for the clamped-free (C-F) beam shown in Fig. 1 are given as

$$u|_{x_1=0} = 0, \quad \left(A^{DFM}\frac{du}{dx_1} - B^{DFM}\frac{d^2w}{dx_1^2}\right)\Big|_{x_1=L} = 0,$$
$$w|_{x_1=0} = 0, \quad \left(-D^{DFM}\frac{d^3w}{dx_1^3} + B^{DFM}\frac{d^2u}{dx_1^2} + F\right)\Big|_{x_1=L} = 0,$$
$$\frac{dw}{dx_1}\Big|_{x_1=0} = 0, \quad \left(-D^{DFM}\frac{d^2w}{dx_1^2} + B^{DFM}\frac{du}{dx_1}\right)\Big|_{x_1=L} = 0. \tag{30}$$

In the above expressions, the parameter F is the point force applied at the free-end of the cantilever beam as indicated in Fig. 1. Solving the governing equations given in Eq. (27) along with the boundary conditions provided in Eq. (30), the following expressions for the mid-plane axial displacement $u(x_1)$, the mid-plane transverse displacement $w(x_1)$, and the magnetic potential difference $\Delta\psi$ induced across the thickness of the beam may be derived

$$u(x_1) = \frac{F}{2\overline{D}^{DFM}}\frac{B^{DFM}}{A^{DFM}}x_1(x_1 - 2L),$$
$$w(x_1) = \frac{F}{6\overline{D}^{DFM}}x_1^2(x_1 - 3L), \tag{31}$$
$$\Delta\psi(x_1) = h\frac{F}{\overline{D}^{DFM}}\left[\frac{C_{11}\mu_{31}}{a_{33}C_{11} + (d_{31})^2}\right](L - x_1),$$

where

$$\overline{D}^{DFM} = D^{DFM} - \frac{(B^{DFM})^2}{A^{DFM}} = I_f\left[C_{11} + \frac{(d_{31})^2}{a_{33}}\right] + A_f\left[g_{31} + \frac{(\mu_{31})^2 C_{11}}{a_{33}C_{11} + (d_{31})^2}\right]. \tag{32}$$

The bending-extension coupling due to FM causing a non-zero $u(x_1)$ may be observed from Eq. (31). Also, the contribution of FM to the rigidity coefficients may be noted from Eq. (28) resulting in modified mechanical responses. Furthermore, the magnetic potential induced across the thickness is also modified due to the direct FM effect.

In the above results, neglecting the PM effect we would get the magneto-elastic response fields to be

$$u(x_1)|_{(d_{31}=0)} = 0,$$
$$w(x_1)|_{(d_{31}=0)} = \frac{F}{6\widetilde{D}^{DFM}}x_1^2(x_1 - 3L), \tag{33}$$
$$\Delta\psi(x_1) = h\frac{F}{\widetilde{D}^{DFM}}\left(\frac{\mu_{31}}{a_{33}}\right)(L - x_1),$$

where

$$\widetilde{D}^{DFM} = I_f C_{11} + A_f \left[g_{31} + \frac{(\mu_{31})^2}{a_{33}} \right]. \tag{34}$$

Thus, a non-zero ME coupling may be noted here from the results for the transverse displacement being modified by a non-zero FM coefficient, and a non-zero magnetic potential being induced by the direct FM effect. Therefore, a ME coupling without the use of the PM materials may be noted from the current study.

B. Converse effect

Having solved the magneto-elastic response for the direct effect, we proceed with the study for a converse effect configuration with magnetic potentials being applied at the surfaces as illustrated in Fig. 1. Thus, the boundary conditions for the magnetic potential are given by

$$\psi(x_3 = h/2) = \Psi_1, \quad \psi(x_3 = -h/2) = 0. \tag{35}$$

Solving the governing equation for the magnetic variables in Eq. (19) using the constitutive relations for B_3 in Eq. (13), definition of H_3 in Eq. (3), and the boundary conditions given above results in the following result for the potential distribution $\psi(x_1, x_3)$ across the domain

$$\psi = -\frac{d_{31}}{2a_{33}} \frac{d^2 w}{dx_1^2} \left(x_3^2 - \frac{h^2}{4} \right) + \frac{\Psi_1}{h} \left(x_3 + \frac{h}{2} \right). \tag{36}$$

Thereby, the magnetic field H_3 is given as

$$H_3 = \frac{d_{31}}{a_{33}} \frac{d^2 w}{dx_1^2} x_3 - \frac{\Psi_1}{h}. \tag{37}$$

The stresses σ_{11} and τ_{311} for the above magnetic field may be written as

$$\begin{aligned} \sigma_{11} &= C_{11} \frac{du}{dx_1} - x_3 \frac{d^2 w}{dx_1^2} \left[C_{11} + \frac{(d_{31})^2}{a_{33}} \right] + \frac{\Psi_1}{h} d_{31}, \\ \tau_{311} &= -g_{31} \frac{d^2 w}{dx_1^2} - x_3 \frac{d^2 w}{dx_1^2} \frac{\mu_{31} d_{31}}{a_{33}} + \frac{\Psi_1}{h} \mu_{31}. \end{aligned} \tag{38}$$

A non-zero increment in the higher order stress τ_{311} is induced by the applied magnetic potential. This response to an applied potential is the converse flexomagnetic effect, in line with the converse piezomagnetic effect causing an additional σ_{11} due to the applied magnetic potential. Following the procedure implemented previously for direct FM effect, we evaluate the stress resultants and thereafter derive the governing equations and the associated boundary conditions for studying the converse effect.

The stress resultants N_{11}, M_{11}, and T_{311} for the converse effect evaluated using the definitions in Eq. (16) and the stresses in Eq. (38) are

$$\begin{aligned} N_{11} &= C_{11} A_f \frac{du}{dx_1} + d_{31} A_f \frac{\Psi_1}{h}, \\ M_{11} &= -I_f \frac{d^2 w}{dx_1^2} \left[C_{11} + \frac{(d_{31})^2}{a_{33}} \right], \\ T_{311} &= -g_{31} A_f \frac{d^2 w}{dx_1^2} + \frac{\Psi_1}{h} A_f \mu_{31}. \end{aligned} \tag{39}$$

The governing equations are derived to be

$$A^{CFM} \frac{d^2 u}{dx_1^2} = 0, \quad -D^{CFM} \frac{d^4 w}{dx_1^4} = 0, \tag{40}$$

where the coefficients axial rigidity A^{CFM} and bending rigidity D^{CFM} of the FM under the converse FM effect are given as

$$A^{CFM} = C_{11} A_f, \quad D^{CFM} = I_f \left[C_{11} + \frac{(d_{31})^2}{a_{33}} \right] + A_f g_{31}. \tag{41}$$

The effect of SGE on bending rigidity, noted in direct effect, is also present here. However, as noted above, the contribution of FM to D^{CFM} is observed to be absent. Moreover, the bending-extension coupling experienced in direct effect configuration is also absent here. The associated boundary conditions for the C-F beam in the current configuration from Eq. (18) are given by

$$u|_{x_1=0} = 0, \quad \left(A^{CFM} \frac{du}{dx_1} + d_{31} A_f \frac{\Psi_1}{h} \right) \Big|_{x_1=L} = 0, \tag{42a}$$

$$w|_{x_1=0} = 0, \quad \left(-D^{CFM} \frac{d^3 w}{dx_1^3} + F \right) \Big|_{x_1=L} = 0, \tag{42b}$$

$$\frac{dw}{dx_1}\Big|_{x_1=0} = 0, \quad \left(-D^{CFM} \frac{d^2 w}{dx_1^2} + A_f \frac{\mu_{31}}{a_{33}} \frac{\Psi_1}{h} \right) \Big|_{x_1=L} = 0. \tag{42c}$$

For an applied potential difference across the thickness, a non-zero moment produced by the flexo-magnetic coupling may be noted in the natural boundary condition corresponding to dw/dx_1 given above in Eq. (42c). This may be referred to as a relaxation moment due to the FM effect. Solving the governing equations given in Eq. (40) along with the boundary conditions provided in Eq. (42) results in the following expressions for the mid-plane values of the axial displacement $u(x_1)$ and transverse displacement $w(x_1)$ of the ferromagnetic beam

$$\begin{aligned} u(x_1) &= -\frac{d_{31}}{C_{11}} \frac{\Psi_1}{h} x_1, \\ w(x_1) &= \frac{F}{6D^{CFM}} x_1^2 (x_1 - 3L) + A_f \frac{\mu_{31}}{2D^{CFM}} \frac{\Psi_1}{h} x_1^2. \end{aligned} \tag{43}$$

Additional transverse displacement caused due to the relaxation-moment caused by the flexomagnetic coupling may be observed in the expressions given above. Similar to the observations for the direct effect configuration, upon

ignoring the PM effect, the axial displacement would be zero. However, the magneto-elastic coupling is evident from the expression for the transverse displacement. Thus, a converse ME coupling even without the use of PM materials can be observed from the current study. Using the above derived result for the transverse displacement in Eq. (36), we get the total potential distribution across the domain as

$$\psi = -\frac{d_{31}}{2a_{33}}\left[\frac{F}{D^{CFM}}(x_1 - L) + \frac{A_f\mu_{31}}{(D^{CFM})}\frac{\Psi_1}{h}\right]\left(x_3^2 - \frac{h^2}{4}\right) + \frac{\Psi_1}{h}\left(x_3 + \frac{h}{2}\right). \tag{44}$$

The contribution of the FM to the effective bending rigidity under the direct effect given in Eq. (32) may be written as

$$\overline{D}_{FM}^{DFM} = A_f\,\frac{(\mu_{31})^2 C_{11}}{a_{33}C_{11} + (d_{31})^2}. \tag{45}$$

However, as mentioned above, the contribution of FM to the bending rigidity under the converse effect is noted to be absent, for the current formulation. Given a_{33} is greater than zero it may be shown that, $D^{DFM} > D^{CFM}$ which indicates that the bending rigidity of the beam under a converse effect is lower than that under direct effect. Moreover, the coupling coefficient B^* for the converse effect is equal to zero.

IV. RESULTS AND DISCUSSION

The analytical results derived above will be numerically analyzed here for quantitatively illustrating the effect of FM over the response of the PM nanobeam. A $CoFe_2O_4$ cantilever beam is chosen for the current study, with a downward point force of $F = 1$ nN being applied at the free end, as depicted in the schematic. The geometric parameters are varied for each study and mentioned wherever necessary. The material properties of $CoFe_2O_4$ necessary for this study are as follows:[55–57]

$$C_{11} = 286\text{GPa}, \quad C_{44} = 45.3\text{GPa},$$
$$a_{33} = 157 \times 10^{-6}\text{N/A}^2, \quad d_{31} = 580.3\text{N/Am}.$$

The material length constants in order to evaluate the SGE constants are all chosen equal to the lattice parameter for a crystalline structure.[58] The lattice parameter for $CoFe_2O_4$ nanoparticles has been experimentally noted to vary between 8 and 9 Å with temperature.[59] Thus, the length parameters are all chosen such that $l_0 = l_1 = l_2 = 1$ nm. Furthermore, the shear modulus μ necessary for the evaluation of the higher order elasticity constants is considered equal to C_{44} given above.

The flexomagnetic coupling tensor for Mn_3GaN has been evaluated from the density functional theory calculations to be equal to 10^{-4} A.[40] Due to lack of the sufficient literature on evaluation of this parameter, we assume that the FM coupling Q^m for $CoFe_2O_4$ is of the same order as that of Mn_3GaN. Furthermore, we deduced this tensor from the form of coupling between the magnetization and strain gradients, as given in Ref. 40 for estimating the magnetic flux caused by the strain gradients, using a magnetic permeability of free space $\mu_f = 4\pi \times 10^{-7}$ N/A^2.[55–57] Thus, the flexomagnetic constant μ_{31} is evaluated to be approximately equal to 10^{-10} N/A, and is used here, unless otherwise mentioned.

Given the size-dependent nature of the FM effect as noted from Eq. (29), we study the effect of different aspect ratios and varying dimensions for a constant aspect ratio. In all the studies carried out here, the aspect ratios are chosen in such a way that the beams are slender, in keeping with the assumptions involved in applying the Euler-Bernoulli displacement hypothesis.

A. Direct FM effect

Initially, we begin with a slender beam of height $h = 10$ nm and an aspect ratio $L/h = 20$ to study the FM effect over the transverse displacement of the PM beam for the direct FM effect configuration. The transverse displacements of the PM beam considering the FM effect ($w|_{FM\neq 0}$) given in Eq. (31), and neglecting the FM effect ($w|_{FM=0}$) given in Eq. (A2) (in Appendix) are evaluated for different values of μ_{31}. The ratio of these transverse displacements is compared for varying μ_{31} and presented in Fig. 2. As seen from the figure, for low values of μ_{31}, the ratio of the transverse displacement does not change appreciably ($< 0.1\%$) by considering the FM effect. However, the effect of the flexomagnetic coefficient on the transverse displacement becomes significant for $\mu_{31} \geq 10^{-7}$ N/A. The influence of the FM effect on the effective bending rigidity presented analytically in Eq. (32) is significant only for high values of the FM coefficients.

The magnetic potential induced across the thickness by the strain-gradient coupling is also expected to increase with the reducing geometric dimensions of the structure [see Eq. (31)]. The effect of the size-dependent character of the strain gradients over the FM response may be studied by comparing the response for different geometric dimensions of the nanobeam. Figure 3 compares the induced $\Delta\psi$ at the free-end of the cantilever beam for different thickness and aspect ratios with $\mu_{31} = 10^{-10}$ N/A. Foremost, the

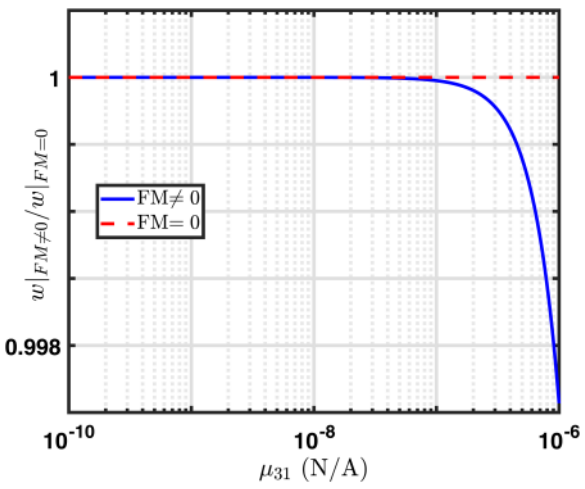

FIG. 2. Comparison of the direct FM effect over variation of the mid-plane transverse displacement at the free-end $w(L)$ for the C-F beam ($h = 10$ nm, $L/h = 20$).

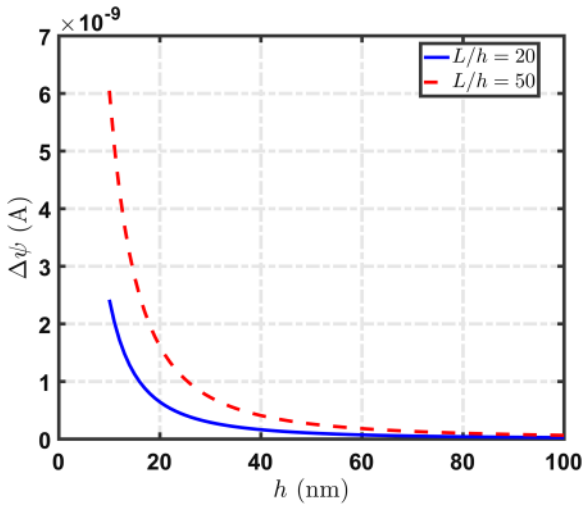

FIG. 3. Variation of the magnetic potential induced across the surfaces, due to the direct FM effect, at the free-end $\Delta\psi(L)$ with respect to thickness of the C-F beam for different aspect ratios.

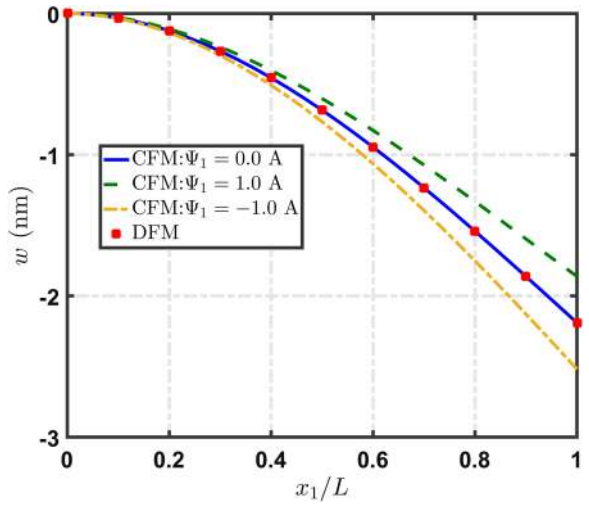

FIG. 4. Mid-plane transverse displacement $w(x_1)$ along length of a C-F beam for varying Ψ_1 due to the converse FM effect ($L = 500$ nm, $L/h = 20$, $F = 1$ nN).

significantly higher magnetic potentials induced in the thinner beam with $L/h = 50$ when compared to the thicker beam with $L/h = 20$ confirms the above notion. Further, the figure indicates that, as the geometric dimensions are increased (height being increased for a particular aspect ratio), the effect of FM coupling over the ME response becomes weaker, as evidenced by the reduced magnetic potential induced across the surfaces.

These studies indicate additional coupling of the magneto-elastic variables in the slender and low-dimensional structures. Also, with a non-zero magnetic potential being induced upon deformation, the FM effect may be used in the development of nanosensors.

B. Converse FM effect

In this section, numerical results due to the converse FM effect are presented using the model derived in Sec. III B. For all the subsequent studies, the FM coefficient is taken to be $\mu_{31} = 10^{-9}$ N/A. The mid-plane transverse displacement for a beam with $L = 500$ nm, and $L/h = 20$, for a non-zero point force applied at the free-end and a magnetic potential Ψ_1 applied at the top surface, is shown in Fig. 4. The difference in the effective bending rigidity for the beam in both configurations (DFM and CFM) is virtually indistinguishable. This may be attributed to low values of μ_{31} thereby the contribution of the FM effect to D^{DFM} being negligible. However, the ME coupling in the converse effect configuration is noted by a change in transverse displacement for a non-zero applied magnetic potential. As discussed previously, this is a result of the restoring moment induced by the FM effect acting along with the moment caused by the downward mechanical load. This may be observed to be acting against the downward mechanical load, thereby reducing the transverse displacement for $\Psi_1 > 0$ in Fig. 4. Also, for $\Psi_1 < 0$, the FM induces a negative moment and adds to moment caused by the external downward force thereby increasing the displacement of the beam.

As noted previously, for the study over the direct FM effect, the influence of the aspect ratio on the converse FM effect, while maintaining $L = 500$ nm, is studied and the results are indicated in Fig. 5. The observations made above regarding the restoring moment by the FM effect for a positive moment are also seen by the reduced numerical value of the displacements for $\Psi_1 > 0$. Comparing the expressions for transverse displacement due to applied force and converse FM from Eq. (43), we get

$$\frac{w|_{F=0}}{w|_{\Psi_1=0}} \propto -\frac{\mu_{31}\Psi_1}{F}\frac{h}{L}. \tag{46}$$

The above comparison confirms the opposing effects of the downward mechanical force, and a positive magnetic potential applied at the top surface over the transverse displacement. Furthermore, the inverse proportionality of the FM effect to the aspect ratio (L/h), noted in the above comparison,

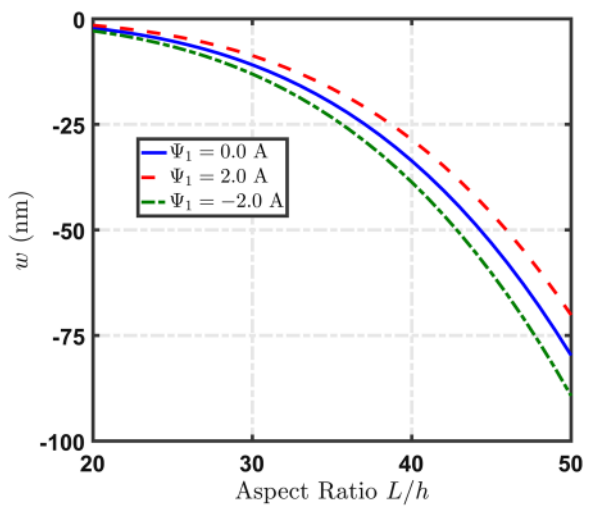

FIG. 5. Variation of mid-plane transverse displacement due to converse FM effect at the free-end $w(L)$ with respect to aspect ratio of the C-F beam for different Ψ_1 ($L = 500$ nm).

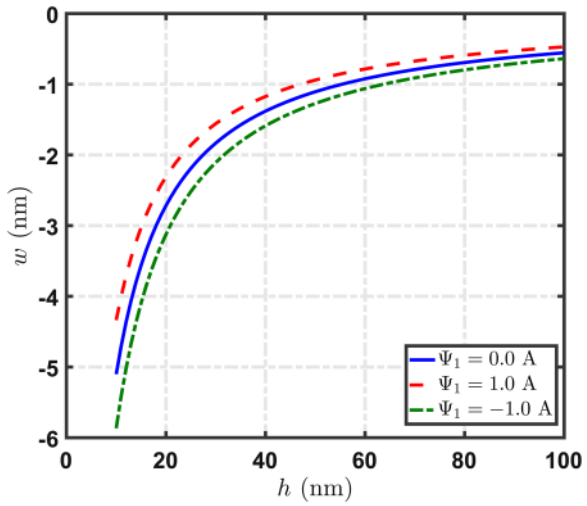

FIG. 6. Variation of mid-plane transverse displacement due to converse FM effect at the free-end $w(L)$ with respect to thickness of the C-F beam for different Ψ_1 ($L/h = 20$).

is confirmed by the reduced effect of the FM for lower aspect ratios in Fig. 5. This is evidenced by the reduced difference in the numerical values for the passive and active transverse displacements in this figure.

Finally, the converse effect of FM on the mechanical response of the cantilever beam of varying dimensions keeping the aspect ratio constant ($L/h = 20$) is indicated in Fig. 6. With the aspect ratio being maintained a constant, the influence of the converse FM effect decreases with increasing dimensions. This indicates the size-dependent behavior of the FM response.

Overall, the results from this study of the converse FM effect point to the potential of the flexomagnetism in the development of smart structures for application as actuators.

V. CONCLUSIONS

In this paper, we have studied the strain-gradient and magnetic field coupling exhibited by ferroics, called the *flexomagnetic* effect. The constitutive relations for this magneto-elastic coupling of the strain gradient tensor and the magnetic field vector have been described by the *flexomagnetic* tensor. The general tensorial form of the governing equations and the associated essential and natural boundary conditions, for the magneto-elastic variables, have been derived from the variational principles. The ME response of a solid considering the flexomagnetic and piezomagnetic effects may be evaluated using these constitutive relations and solving the governing equations with a proper choice of boundary conditions. As an example, we have studied the ME response of a cantilever beam to determine the effect of the flexomagnetism over the piezomagnetic beams. The analytical expressions for the ME response under direct and converse FM effects have been derived here. A quantitative evaluation of these analytical results points to the size-dependent behavior of the FM coupling, which will be of significance in the nanostructures. The potential for flexomagnetic materials in the development of magneto-elastic smart structures without using piezomagnetic materials has also been identified in this study. With these observations, it has been shown that the flexomagnetic effect-based magnetoelastic actuators and sensors may be developed for various applications.

APPENDIX: BENDING RESPONSE OF PM BEAMS

The magneto-elastic constitutive relations of a piezomagnetic beam, while ignoring the flexomagnetic and size-effects, are given as

$$\sigma_{11} = C_{11}\epsilon_{11} - d_{31}H_3, \quad B_3 = a_{33}H_3 + d_{31}\epsilon_{11}. \tag{A1}$$

The magnetic governing equations are the same as derived previously and given in Eq. (19). The associated boundary conditions for the magnetic variables corresponding to the direct and converse PM effect studies are given in Eq. (20). Solving Eq. (19) for these boundary conditions, the expressions for magnetic potential ψ and the transverse magnetic field H_3 may be obtained for both these configurations. Using these expressions in the above constitutive relations, the stress resultants may be evaluated from Eq. (16). Thereby, the mechanical governing equations may be derived and solved for the magneto-elastic response of the piezomagnetic beam. The ME responses due to the direct PM effect are

$$\begin{aligned} u(x_1) &= 0, \quad w(x_1) = \frac{F}{6D}x_1^2(x_1 - 3L), \\ H_3(x_1, x_3) &= \frac{d_{31}}{a_{33}}\frac{F}{D}x_3(x_1 - L), \end{aligned} \tag{A2}$$

where

$$D = \left[C_{11} + \frac{(d_{31})^2}{a_{33}}\right]I_f.$$

The responses for the PM beam due to the converse PM effect for an applied potential, as prescribed in Eq. (35), are

$$\begin{aligned} u(x_1) &= -\frac{d_{31}}{C_{11}}\frac{\Psi_1}{h}x_1, \quad w(x_1) = \frac{F}{6D}x_1^2(x_1 - 3L), \\ \psi(x_1, x_3) &= -\frac{d_{31}}{2a_{33}}\frac{F}{D}\left(x_3^2 - \frac{h^2}{4}\right)(x_1 - L) + \frac{\Psi_1}{h}\left(x_3 + \frac{h}{2}\right). \end{aligned} \tag{A3}$$

[1]D. C. C. Lam, F. Yang, A. C. M Chong, J. Wang, and P. Tong, "Experiments and theory in strain gradient elasticity," J. Mech. Phys. Solids **51**(8), 1477–1508 (2003).
[2]A. W. McFarland and J. S. Colton, "Role of material microstructure in plate stiffness with relevance to microcantilever sensors," J. Micromech. Microeng. **15**(5), 1060 (2005).
[3]N. A. Fleck and J. W. Hutchinson, "Strain gradient plasticity," Adv. Appl. Mech. **33**, 296–361 (1997).
[4]R. D. Mindlin, "Micro-structure in linear elasticity," Arch. Ration. Mech. Anal. **16**(1), 51–78 (1964).
[5]R. D. Mindlin and N. N. Eshel, "On first strain-gradient theories in linear elasticity," Int. J. Solids Struct. **4**(1), 109–124 (1968).
[6]V. S. Mashkevich, "Electrical, optical, and elastic properties of diamond-type crystals. II. Lattice vibrations with calculation of atomic dipole moments," Sov. Phys. JETP **5**(4), 707–713 (1957).
[7]S. M. Kogan, "Piezoelectric effect during inhomogeneous deformation and acoustic scattering of carriers in crystals," Sov. Phys. Solid State **5**, 2069–2070 (1964).
[8]P. Harris, "Mechanism for the shock polarization of dielectrics," J. Appl. Phys. **36**(3), 739–741 (1965).

[9]W. Ma and L. E. Cross, "Large flexoelectric polarization in ceramic lead magnesium niobate," Appl. Phys. Lett. **79**(26), 4420–4422 (2001).
[10]W. Ma and L. E. Cross, "Strain-gradient-induced electric polarization in lead zirconate titanate ceramics," Appl. Phys. Lett. **82**(19), 3293–3295 (2003).
[11]L. E. Cross, "Flexoelectric effects: Charge separation in insulating solids subjected to elastic strain gradients," J. Mater. Sci. **41**(1), 53–63 (2006).
[12]W. Ma and L. E. Cross, "Observation of the flexoelectric effect in relaxor pb (mg 1/3 nb 2/3) o 3 ceramics," Appl. Phys. Lett. **78**(19), 2920–2921 (2001).
[13]W. Ma and L. E. Cross, "Flexoelectric effect in ceramic lead zirconate titanate," Appl. Phys. Lett. **86**(7), 072905 (2005).
[14]W. Ma and L. E. Cross, "Flexoelectricity of barium titanate," Appl. Phys. Lett. **88**(23), 232902 (2006).
[15]P. Zubko, G. Catalan, and A. K. Tagantsev, "Flexoelectric effect in solids," Annu. Rev. Mater. Res. **43**, 387–421 (2013).
[16]Q. Deng, M. Kammoun, A. Erturk, and P. Sharma, "Nanoscale flexoelectric energy harvesting," Int. J. Solids Struct. **51**(18), 3218–3225 (2014).
[17]M. S. Majdoub, P. Sharma, and T. Çağin, "Dramatic enhancement in energy harvesting for a narrow range of dimensions in piezoelectric nanostructures," Phys. Rev. B **78**(12), 121407 (2008).
[18]M. S. Majdoub, P. Sharma, and T. Cagin, "Enhanced size-dependent piezoelectricity and elasticity in nanostructures due to the flexoelectric effect," Phys. Rev. B **77**(12), 125424 (2008).
[19]R. Maranganti, N. D. Sharma, and P. Sharma, "Electromechanical coupling in nonpiezoelectric materials due to nanoscale nonlocal size effects: Green's function solutions and embedded inclusions," Phys. Rev. B **74**(1), 014110 (2006).
[20]R. Maranganti and P. Sharma, "Atomistic determination of flexoelectric properties of crystalline dielectrics," Phys. Rev. B **80**(5), 054109 (2009).
[21]Z. Yan and L. Y. Jiang, "Flexoelectric effect on the electroelastic responses of bending piezoelectric nanobeams," J. Appl. Phys. **113**(19), 194102 (2013).
[22]Z. Yan, "Size-dependent bending and vibration behaviors of piezoelectric circular nanoplates," Smart Mater. Struct. **25**(3), 035017 (2016).
[23]Z. Yan and L. Jiang, "Surface effects on the electromechanical coupling and bending behaviours of piezoelectric nanowires," J. Phys. D Appl. Phys. **44**(7), 075404 (2011).
[24]Z. Yan and L. Jiang, "Size-dependent bending and vibration behaviour of piezoelectric nanobeams due to flexoelectricity," J. Phys. D Appl. Phys. **46**(35), 355502 (2013).
[25]M. C. Ray, "Exact solutions for flexoelectric response in nanostructures," J. Appl. Mech. **81**(9), 091002 (2014).
[26]M. C. Ray, "Enhanced magnetoelectric effect in multiferroic composite beams due to flexoelectricity and transverse deformations," Int. J. Mech. Mater. Des. **14**, 461–472 (2018).
[27]S. Sidhardh, and M. C. Ray, "Exact solutions for flexoelectric response in elastic dielectric nanobeams considering generalized constitutive gradient theories," Int. J. Mech. Mater. Des. (published online).
[28]S. Sidhardh, and M. C. Ray, "Effect of nonlocal elasticity on the performance of a flexoelectric layer as a distributed actuator of nanobeams," Int. J. Mech. Mater. Des. **14**(2), 297–311 (2018).
[29]E. A. Eliseev, A. N. Morozovska, Y. Gu, A. Y. Borisevich, L.-Q. Chen, V. Gopalan, and S. V. Kalinin, "Conductivity of twin-domain-wall/surface junctions in ferroelastics: Interplay of deformation potential, octahedral rotations, improper ferroelectricity, and flexoelectric coupling," Phys. Rev. B **86**(8), 085416 (2012).
[30]E. A. Eliseev, A. N. Morozovska, M. D. Glinchuk, B. Y. Zaulychny, V. V. Skorokhod, and R. Blinc, "Surface-induced piezomagnetic, piezoelectric, and linear magnetoelectric effects in nanosystems," Phys. Rev. B **82**(8), 085408 (2010).
[31]A. Y. Borisevich, E. A. Eliseev, A. N. Morozovska, C.-J. Cheng, J.-Y. Lin, Y.-H. Chu, D. Kan, I. Takeuchi, V. Nagarajan, and S. V. Kalinin, "Atomic-scale evolution of modulated phases at the ferroelectric–antiferroelectric morphotropic phase boundary controlled by flexoelectric interaction," Nat. Commun. **3**, 775 (2012).
[32]A. N. Morozovska, E. A. Eliseev, A. K. Tagantsev, S. L. Bravina, L.-Q. Chen, and S. Kalinin, "Thermodynamics of electromechanically coupled mixed ionic-electronic conductors: Deformation potential, vegard strains, and flexoelectric effect," Phys. Rev. B **83**(19), 195313 (2011).
[33]L. He, J. Lou, A. Zhang, H. Wu, J. Du, and J. Wang, "On the coupling effects of piezoelectricity and flexoelectricity in piezoelectric nanostructures," AIP Adv. **7**(10), 105106 (2017).
[34]S. Sidhardh and M. C. Ray, "Effective properties of flexoelectric fiber-reinforced nanocomposite," Mater. Today Commun. **17**, 114–123 (2018).
[35]Y. P. Bobylev and S. A. Pikin, Pis'Ma Zh. Tekh. Fiz. (Sov. Tech. Phys. Lett.) **5**, 1032 (1979).
[36]A. P. Pyatakov and A. K. Zvezdin, "Flexomagnetoelectric interaction in multiferroics," Eur. Phys. J. B **71**(3), 419–427 (2009).
[37]L. D. Landau, J. S. Bell, M. J. Kearsley, L. P. Pitaevskii, E. M. Lifshitz, and J. B. Sykes, *Electrodynamics of Continuous Media* (Elsevier, 2013), Vol. 8.
[38]Z.-G. Ban, S. P. Alpay, and J. V. Mantese, "Fundamentals of graded ferroic materials and devices," Phys. Rev. B **67**(18), 184104 (2003).
[39]S. P. Alpay, I. B. Misirlioglu, A. Sharma, and Z.-G. Ban, "Structural characteristics of ferroelectric phase transformations in single-domain epitaxial films," J. Appl. Phys. **95**(12), 8118–8123 (2004).
[40]E. A. Eliseev, M. D. Glinchuk, V. Khist, V. V. Skorokhod, R. Blinc, and A. N. Morozovska, "Linear magnetoelectric coupling and ferroelectricity induced by the flexomagnetic effect in ferroics," Phys. Rev. B **84**(17), 174112 (2011).
[41]E. A. Eliseev, A. N. Morozovska, M. D. Glinchuk, and R. Blinc, "Spontaneous flexoelectric/flexomagnetic effect in nanoferroics," Phys. Rev. B **79**(16), 165433 (2009).
[42]E. A. Eliseev, "Complete symmetry analyses of the surface-induced piezomagnetic, piezoelectric and linear magnetoelectric effects," Ferroelectrics **417**(1), 100–109 (2011).
[43]P. Lukashev and R. F. Sabirianov, "Flexomagnetic effect in frustrated triangular magnetic structures," Phys. Rev. B **82**(9), 094417 (2010).
[44]P. Lukashev and R. F. Sabirianov, "Spin density in frustrated magnets under mechanical stress: Mn-based antiperovskites," J. Appl. Phys. **107**(9), 09E115 (2010).
[45]S. Shen and S. Hu, "A theory of flexoelectricity with surface effect for elastic dielectrics," J. Mech. Phys. Solids **58**(5), 665–677 (2010).
[46]M. E. Lines and A. M. Glass, *Principles and Applications of Ferroelectrics and Related Materials* (Oxford University Press, 1977).
[47]R. Wang, Q. Han, and E. Pan, "An analytical solution for a multilayered magneto-electro-elastic circular plate under simply supported lateral boundary conditions," Smart Mater. Struct. **19**(6), 065025 (2010).
[48]J. Liu, P. Zhang, G. Lin, W. Wang, and S. Lu, "Solutions for the magneto-electro-elastic plate using the scaled boundary finite element method," Eng. Anal. Bound. Elem. **68**, 103–114 (2016).
[49]S. Sidhardh and M. C. Ray, "Exact solutions for elastic response in micro- and nano-beams considering strain gradient elasticity," Math. Mech. Solids (published online).
[50]A. S. Yurkov, "Elastic boundary conditions in the presence of the flexoelectric effect," JETP Lett. **94**(6), 455–458 (2011).
[51]S. Santapuri, R. L. Lowe, S. E. Bechtel, and M. J. Dapino, "Thermodynamic modeling of fully coupled finite-deformation thermo-electro-magneto-mechanical behavior for multifunctional applications," Int. J. Eng. Sci. **72**, 117–139 (2013).
[52]X.-J. Xu, Z.-C. Deng, K. Zhang, and J.-M. Meng, "Surface effects on the bending, buckling and free vibration analysis of magneto-electro-elastic beams," Acta Mech. **227**(6), 1557–1573 (2016).
[53]R. Omidian, Y. Beni, and F. Mehralian, "Analysis of size-dependent smart flexoelectric nanobeams," Eur. Phys. J. Plus **132**(11), 481 (2017).
[54]S. Zhou, A. Li, and B. Wang, "A reformulation of constitutive relations in the strain gradient elasticity theory for isotropic materials," Int. J. Solids Struct. **80**, 28–37 (2016).
[55]E. Pan, "Exact solution for simply supported and multilayered magneto-electro-elastic plates," J. Appl. Mech. **68**(4), 608–618 (2001).
[56]E. Pan and P. Heyliger, "Exact solutions for magneto-electro-elastic laminates in cylindrical bending," Int. J. Solids Struct. **40**(24), 6859–6876 (2003).
[57]E. Pan and F. Han, "Exact solution for functionally graded and layered magneto-electro-elastic plates," Int. J. Eng. Sci. **43**(3–4), 321–339 (2005).
[58]R. Maranganti and P. Sharma, "Length scales at which classical elasticity breaks down for various materials," Phys. Rev. Lett. **98**(19), 195504 (2007).
[59]C. R. Stein, M. T. S. Bezerra, G. H. A. Holanda, J. André-Filho, and P. C. Morais, "Structural and magnetic properties of cobalt ferrite nanoparticles synthesized by co-precipitation at increasing temperatures," AIP Adv. **8**(5), 056303 (2018).